communications journals

Supplementary Information for

Insights into volcanic unrest by correlating petrological and seismic observations at Kizimen (Kamchatka, Russia)

Lea Ostorero[1*], Hélène Balcone-Boissard[2], Georges Boudon[1], Nikolai M. Shapiro[3,4], Alexander Belousov[5], Marina Belousova[5], Andreas Auer[6], Sergey L. Senyukov[7], Svetlana Ya. Droznina[7]

[1]Université de Paris, Institut de physique du globe de Paris, CNRS, F-75005 Paris, France
[2]Institut des Sciences de la Terre de Paris (ISTeP), UMR 7193, CNRS-Sorbonne Université, Paris, France
[3]Institut des Sciences de la Terre (ISTerre), Université Grenoble Alpes, CNRS, 38400, Grenoble, France
[4]Schmidt Institute of Physics of the Earth, Russian Academy of Sciences, 10 B. Gruzinskaya St., Moscow, 123995
[5]Institute of Volcanology and Seismology, 9 Piip Boulevard, Petropavlovsk-Kamchatksy, Kamchatsky region 683006, Russia
[6]Department of Geoscience, Shimane University, 1060 Nishikawatsu, Matsue 690-8504, Japan
[7]Kamchatka Branch of the Geophysical Survey, Russian Academy of Sciences, 9 Piip Boulevard, Petropavlovsk-Kamchatksy, Kamchatsky region 683006, Russia

Corresponding author: Lea Ostorero.
Email: ostorero@ipgp.fr

Supplementary Note

Whole rocks. The 2010-2013 magmas have whole rock compositions in the andesitic field, with 58-60 wt% SiO_2 and 4.8-5 wt% Na_2O +K_2O (recalculated with total iron as FeO and on anhydrous basis) and in the dacitic field, with a composition of 64 wt% SiO_2 and 5.6 wt% Na_2O +K_2O (**Supplementary Table 1**). The compositions of the samples are in the same domain as in a previous study[1]. Samples are porphyritic: ~36% of crystals for the hybrids and ~29% of crystals for the dacite (the crystallinities of the samples have been estimated after a vesicle-free estimation by point counting on thin sections of the hybrids and dacite samples thanks to Mesurim (Version 3.4; http://acces.ens-lyon.fr/acces/logiciels/applications/mesurim)).

Orthopyroxene zonations: types and proportions. 1832 orthopyroxene (opx) crystals were studied for the 2010-2013 eruption. We analyzed them using a scanning electron microscope and electron probe microanalyzer (EPMA). Zoned crystals were classified according to the type of zonation observed: either a single one (normal or reverse zonation) or a multiple one (**Supplementary Figure 2**). In both dacite and andesite, the proportions of unzoned crystals are higher than zoned ones (66% and 67% of unzoned crystals respectively; **Supplementary Figure 2**). Only 31-32% of them are zoned, with a majority of normal-zoned opx in the dacite while reverse-zoned opx in the andesite are more represented (**Supplementary Figure 2**). Multiple-zoned opx represent a small proportion of zoned crystals (3-6%) and are mainly reverse-zoned then normal-zoned, from core to rim (**Supplementary Figure 2**). Some opx also show reactional borders or remelting textures and represent a few % of the opx population (**Supplementary Figure 2**).

Orthopyroxene zonations: compositions. Profiles in zoned opx were mainly acquired in normal-zoned opx for the dacite and reverse-zoned opx for the andesite with the EPMA (37 for the dacite and 75 for the andesite) (**Supplementary Data 1**). Unzoned opx compositions were also acquired (41 for the dacite and 67 for the andesite) (**Supplementary Data 1 and Supplementary Figure 3**).
The range of compositions displays no systematic differences for the cores of the unzoned and zoned opx of both samples (En_{62-64}; Enstatite content ($\mathbf{En} = \frac{\mathbf{Mg}}{\mathbf{Mg+Fe}}$)). But the singly normal-zoned rims of the dacite show lower Enstatite content (En_{44-54}) compared to singly reverse-zoned rims with higher En content of the andesite opx (En_{64-73}) (**Supplementary Data 1; Supplementary Figure 3**).
For multiple-zoned ones, they mainly show first a reverse path and then a normal one (**Supplementary Data 1; Supplementary Figure 3**). Microlites in the andesitic samples are between En_{63-72} (**Supplementary Data 1**). Cores of opx with remelting textures in the dacite have the same compositions as the other opx while the ones in the andesite have compositions from En_{65-73} (**Supplementary Data 1**). The magma dynamics with En analysis of the opx are the subject of another study.

Timescales. Timescales have been modelled on the most representative opx zonations based on **Supplementary Figure 2**. For the dacites, timescales are around 1-6 years for the normal-zoned crystals, with 80% of them between 1-2 years (**Supplementary Figure 4**). For the multiple-zoned opx, the bulk of the timescales are also younger than 2 years

(for the inner rims (reverse or normal-zoned): timescales between 1-5 years, and for the outer rims: some timescales longer than 24 years; **Supplementary Figure 4; Supplementary Data 3**).
For the andesites, the timescales are distributed between 1 to 4 years for the single reversely-zoned crystals, with 90% of them between 1-2 years before the eruption (**Supplementary Figure 4**). Normal-zoned crystals give two timescales between 1 to 11 years (**Supplementary Figure 4**). For the multiple-zoned crystals, the bulk of the analyses also represent the final 2 years pre-eruption, with little uncertainties (3 inner rims between 1-8 years and one inner reverse-zoned rim gives a timescale of 62 years; for the outer ones, 4 reverse-zoned ones are ~1 year and two normal ones are between 2-23 years**; Supplementary Figure 4; Supplementary Data 3**).

Magma temperatures estimation. Equilibrium temperatures were calculated from the compositions of touching pairs of titanomagnetite and ilmenite (mgt/ilm) following a numerical model[2] (**Supplementary Data 2**). A mean temperature of 832 ± 37 °C and 847 ± 57 °C were calculated for the dacite (on 3 pairs) and andesite (on 23 pairs) respectively (where the number that follows the ± sign is a standard deviation; **Supplementary Data 2**).
A temperature of 874 °C has also been estimated thanks to the plag/liquid thermometer (equation 24a)[3], knowing an estimation of the pressure[1], as well as host and melt inclusion compositions.

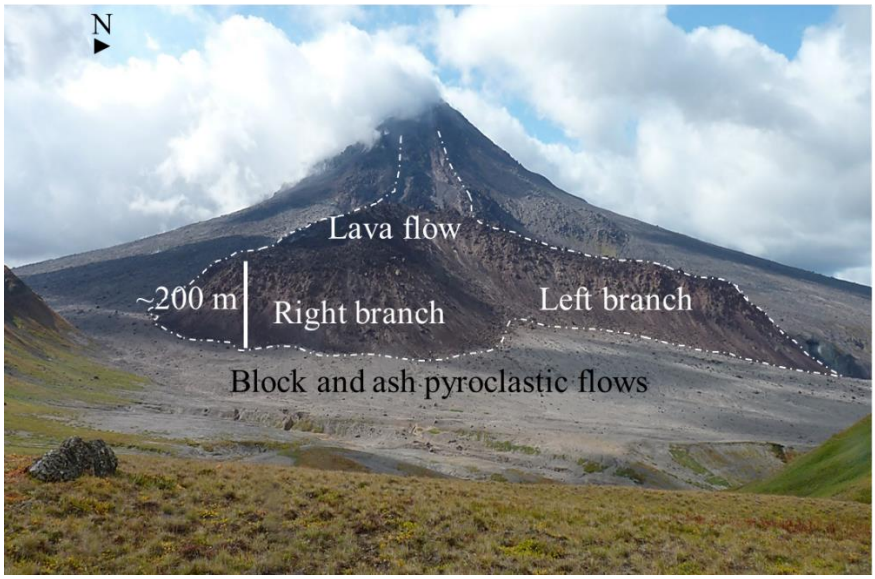

Supplementary Figure 1. Kizimen volcano in Kamchatka. Picture of Kizimen (taken in August 2019), showing the block and ash pyroclastic flows deposits and the lava flow from the 2010-2013 eruption with two branches.

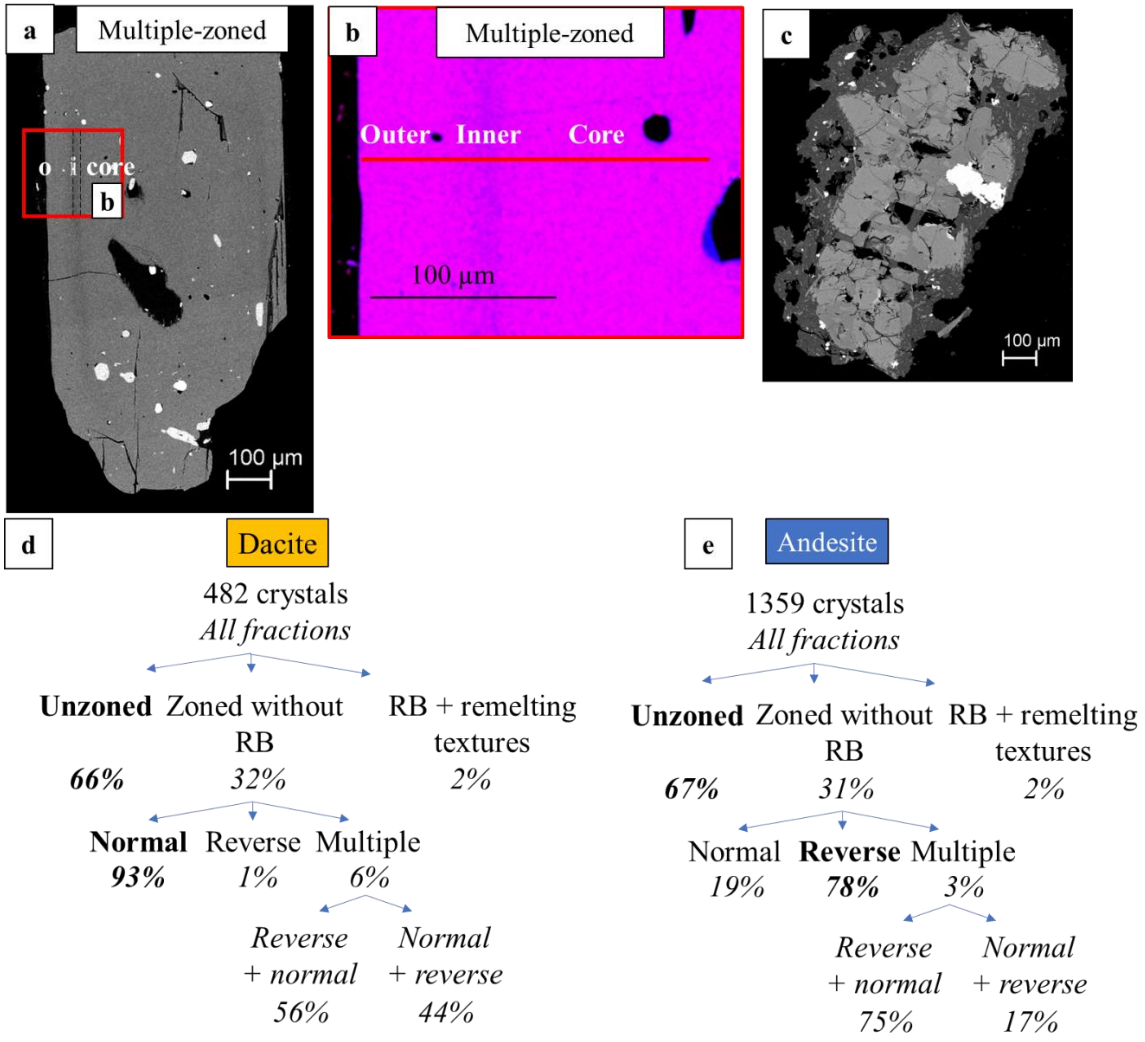

Supplementary Figure 2. Minor textures identified in the opx and proportions of the different zonations in the opx populations in the dacite and andesite. a) Multiple-zoned opx, either reverse + normal (as the image) or normal + reverse from the core to the rim; **b)** High-resolution image of the multiple-zoned opx in **a);** chemical map in RGB colors done with the SEM at Sorbonne Université: Fe and Mg images merged with *ImageJ* (https://imagej.nih.gov/ij/; version 1.52a). The inner/outer rims are shown; **c)** Opx with reactional borders (RB) and remelting textures; **d)** Proportions of the zonations identified in the opx of the dacite in all fractions (500-710 µm, 355-500, 250-355 and 125-250 µm); RB: reactional borders and **e)** in the opx of the andesitic samples.

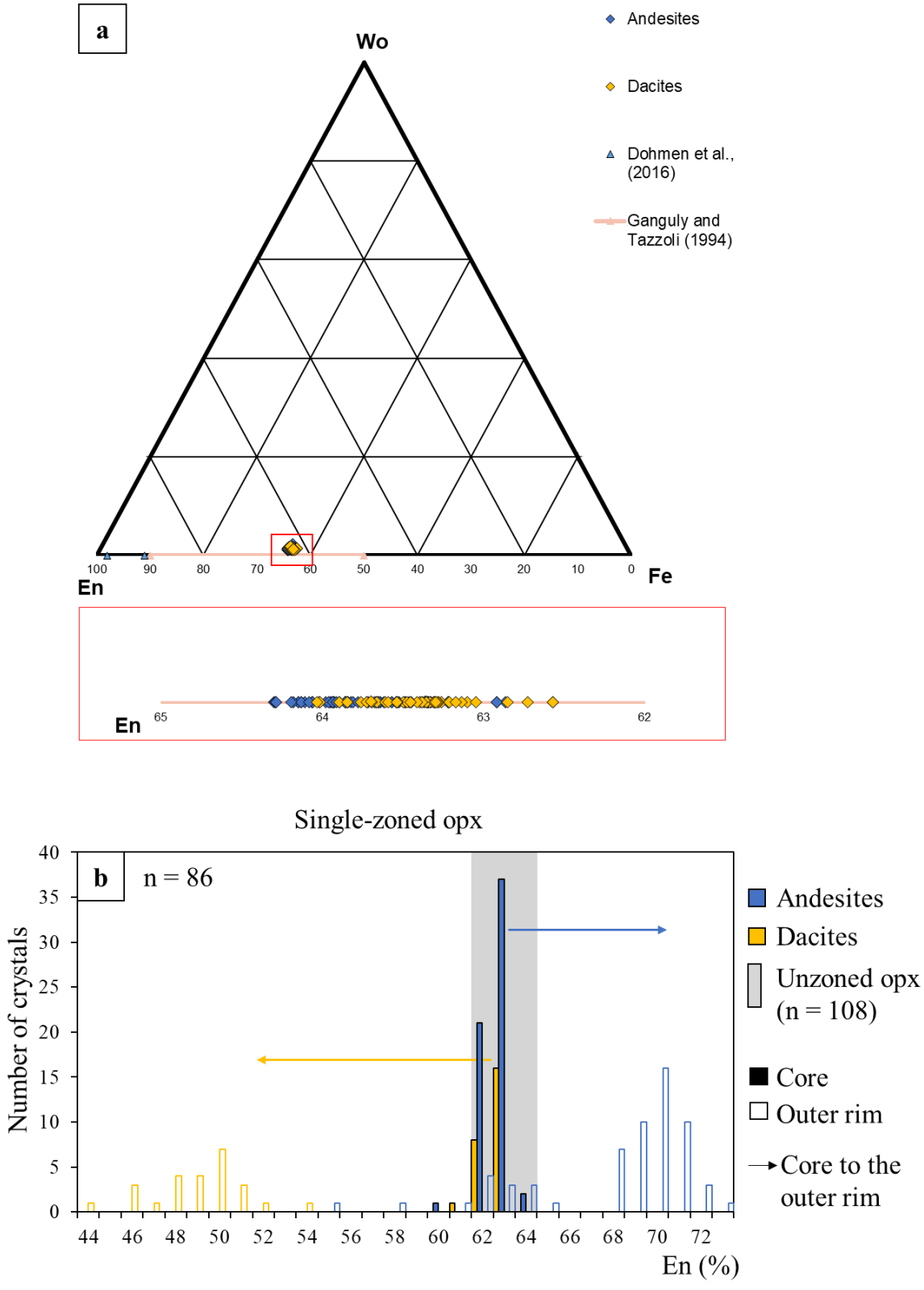

Supplementary Figure 3. Orthopyroxenes En contents (%). a) Ternary diagram of the unzoned opx compositions of the dacite and andesite samples from Kizimen 2010-2013

eruption, with the three poles (Wollastonite (Wo), Enstatite (En) and Ferrosilite (Fs)); Red Square: Zoom on the opx compositions. In orange: En contents domain for which the Fe-Mg interdiffusion coefficient parametrization is formulated[4]. **b)** Frequency histogram of the En content of unzoned and single-zoned opx of the 2010-2013 eruption (unzoned opx in the grey zone). The arrows underline the major path from the core to the rim recorded by the single-zoned opx. The number of opx analyzed is specified (n). The cores of the zoned opx are in the same range as the unzoned opx.

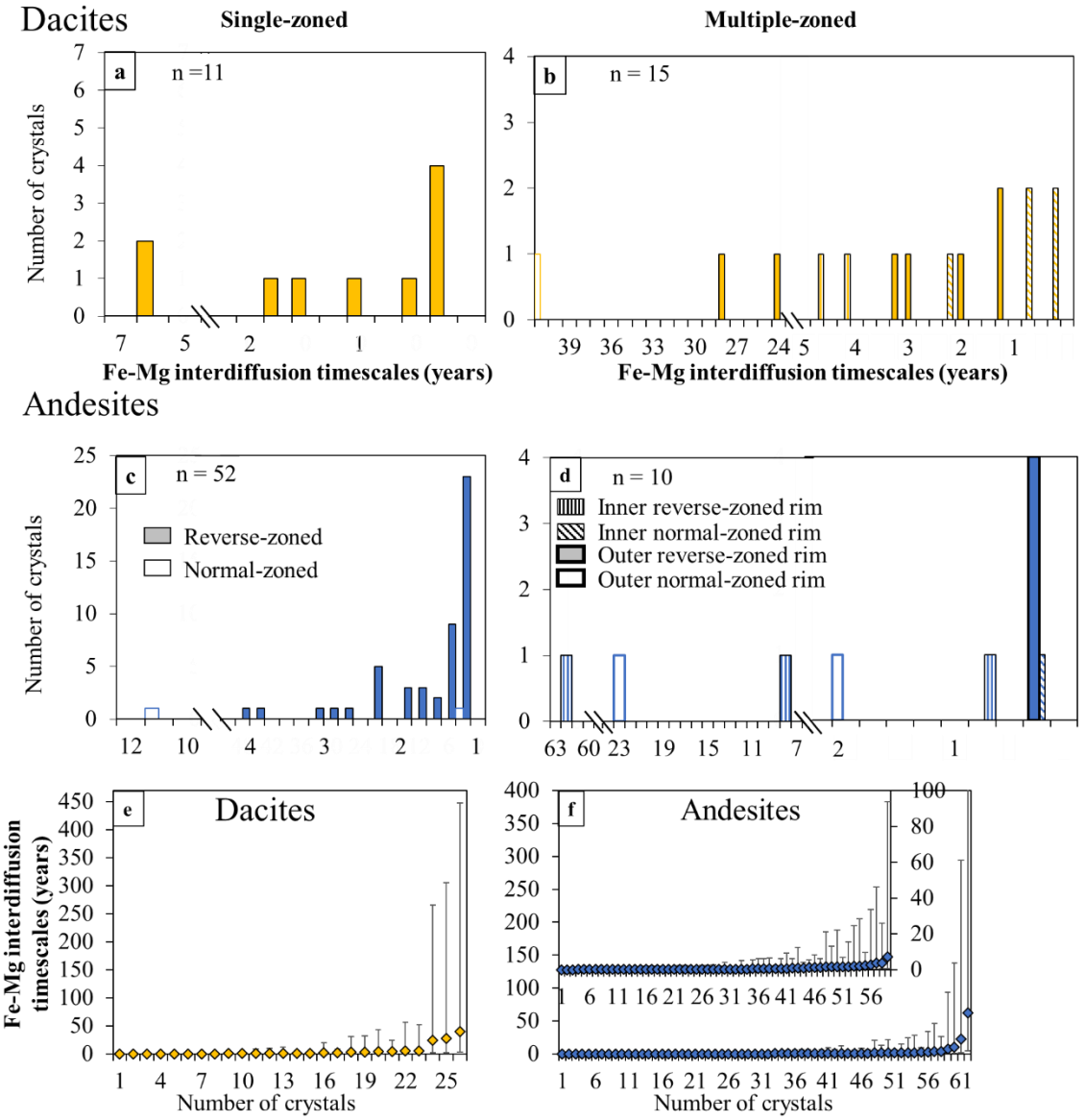

Supplementary Figure 4. Frequency histograms of Fe-Mg interdiffusion timescales modelled in opx at 832 ± 37 °C for the dacite (a-b) and 847 ± 57 °C for the andesite (c-d) for core-rim and inner-outer rim boundaries of single-zoned (SZ) and multiple-zoned (MZ) opx; (e-f) individual timescales and their absolute uncertainties are based on the propagation of a temperature uncertainty of ± 37 °C for the dacite or 57 °C for the andesite and uncertainties associated to SEM images are presented. The type of zonation is specified (reverse-zoned or normal-zoned). The timescales are presented as times before the eruptions and can be found in **Supplementary Data 3**. n is the number of profiles modelled (in SZ, MZ opx). These uncertainties are due to the diffusivity calculations (D_0, the interdiffusion coefficient, the activation energy E_a), temperature and resolution of grayscale values of the BSE images[5,6] and are calculated thanks to a Monte Carlo simulation. These uncertainties are asymmetric, with a larger positive error bar and a smaller negative error bar, due to the logarithmic effect of the uncertainties on mainly temperature and diffusivity calculations[7]. The error bars show a high variability, especially

for the longest timescales, which places a limit on the statistics of the modelled timescales and their significance[8].

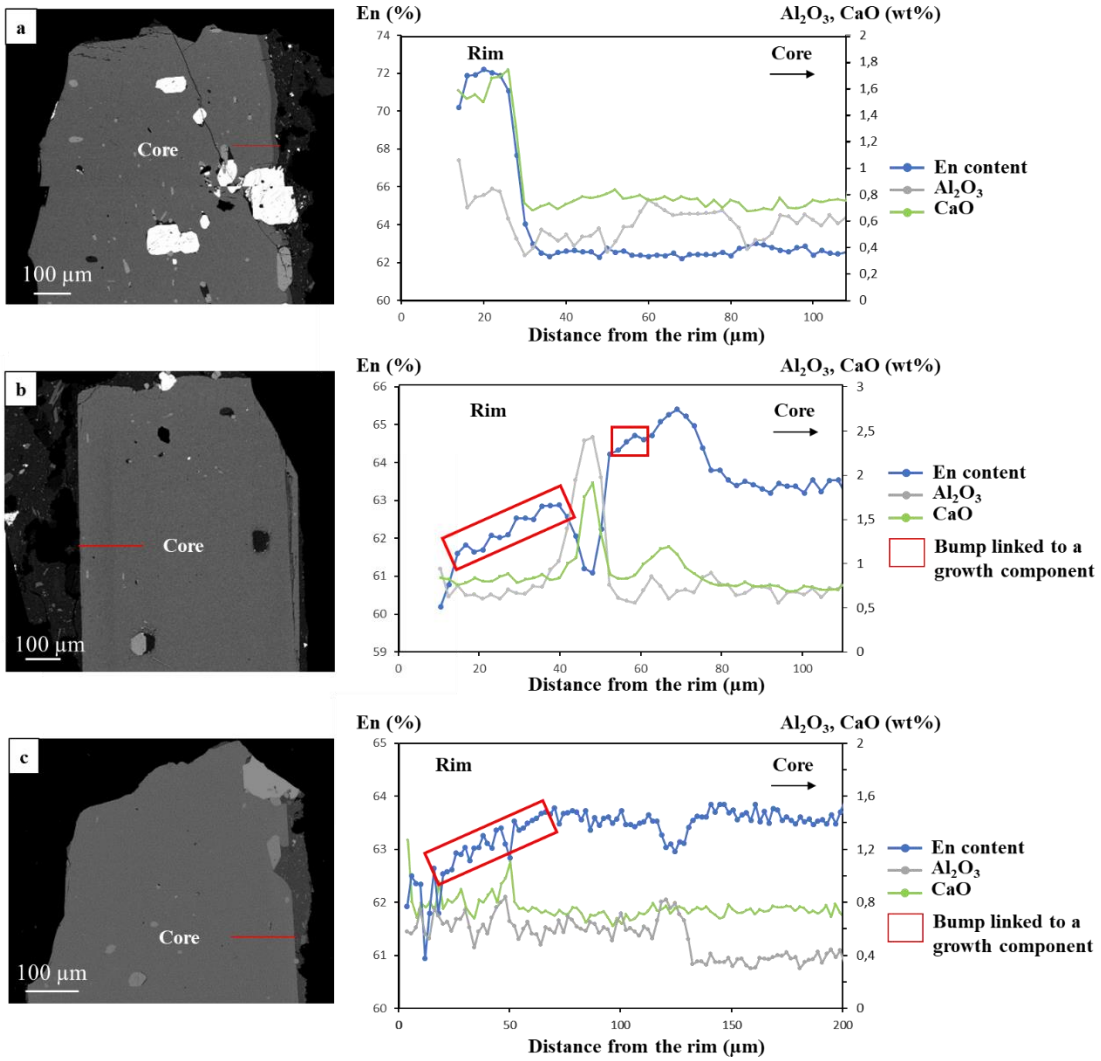

Supplementary Figure 5. Scanning electron microscope images and En content (blue) (%), Al_2O_3 (grey) and CaO content (green) (wt%) of zoned opx. a) SEM image of a reverse-zoned opx and its associated diffusion profile with a shape close to an ideal diffusion sigmoid, without bumps linked to a growth component or distortion. Al_2O_3 (grey) is slightly offset compared to the En content (%). b) SEM image of a multiple-zoned opx showing bumps and not a linear compositional plateau and showing for the outermost rim, no variations in Al_2O_3 (grey) and CaO (green). As Al and Ca diffuse slower than Fe-Mg in opx[9–12] and as no transition zone in Al and Ca are recorded for this rim, this outer rim seems to have been affected by growth and is not modelled to find a timescale. c) SEM image of a multiple-zoned opx with a normal-zoned outer rim that shows peaks and bumps with a growth effect and not an ideal sigmoid. Furthermore, Al_2O_3 (grey) and CaO (green) contents do not show transition zones.

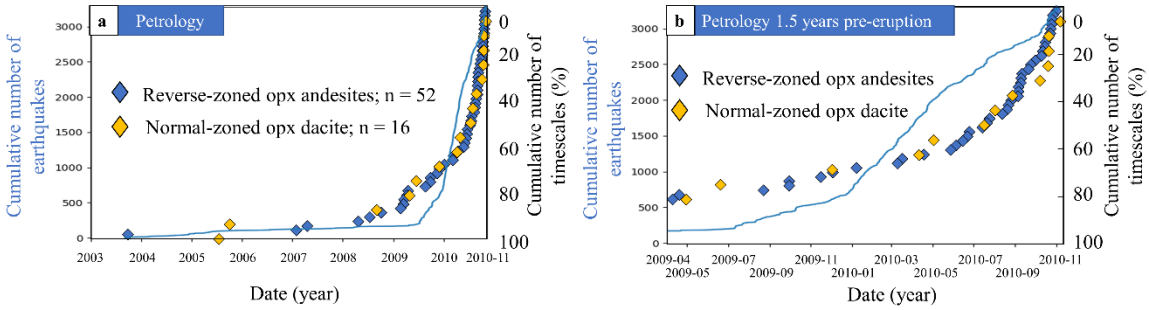

Supplementary Figure 6. Cumulative number of the timescales estimated on the major compositional changes evidenced for the andesite and dacite (reverse zoning for the andesite and normal zoning for the dacite; Supplementary Data 3) and cumulative number of earthquakes. a) From January 2003 to the time of eruption (11/11/20210); **b)** Focus on the 1.5 years pre-eruption. We observe a correlation between the timescales modelled and the cumulative number of earthquakes. See **Figure 2** for the comparison with the depth of the earthquakes.

Sample	K5 (KIZI 5)	K6 (KIZI 6)	K8 (KIZI 8)	K9 (KIZI 9)
Nature	Andesite	Dacite	Andesite	Andesite
SiO_2 (wt%)	58,91	63,56	56,97	57,56
TiO_2 (wt%)	0,73	0,60	0,82	0,81
Al_2O_3 (wt%)	17,02	16,11	17,23	17,36
Fe_2O_3 (wt%)	7,30	5,69	8,14	7,99
MnO (wt%)	0,15	0,12	0,16	0,15
MgO (wt%)	3,16	2,38	3,51	3,42
CaO (wt%)	6,71	5,48	7,18	7,13
Na_2O (wt%)	3,60	3,76	3,49	3,56
K_2O (wt%)	1,37	1,74	1,22	1,23
P_2O_5 (wt%)	0,16	0,15	0,17	0,17
LOI (wt%)	0,14	0,05	0,35	0,03
Total	99,23	99,63	99,23	99,41

Supplementary Table 1. Whole rock major elements. The sampling locations are specified in **Supplementary Table 2**. Analyses have been performed at CRPG (Centre de Recherches Pétrographiques et Géochimiques, Nancy, France) by ICP-OES (Inductively Coupled Plasma-Optical Emission Spectrometry)[13]. The type of deposit is specified. Data are expressed with total Fe as Fe^{3+} with LOI detailed.

Sample	Localisation	Coordinates	Nature of the sample
Kizi 5	Block and ash flow 2010-2013	N55°08.044', E160°22.310'	Andesite
Kizi 6	Block and ash flow 2010-2013 (1074 m)	N55°08.287', E160°22.041'	Dacite
Kizi 8	Block and ash flow 2010-2013 (1175 m)	N55°08.008', E160°22.178	Andesite
Kizi 9	Block and ash flow 2010-2013 (1169 m)	N55°07.991', E160°22.209'	Andesite
Kizi 16	Block and ash flow 2010-2013 (1105 m)	N 55°07.802', E160°22.986'	Banded samples

Supplementary Table 2. Description of the 2010-2013 eruptions of Kizimen samples studied here (localization, coordinates and nature of the samples are specified).

Supplementary Data 1-3 (separate files).

References

1. Auer, A., Belousov, A. & Belousova, M. Deposits, petrology and mechanism of the 2010–2013 eruption of Kizimen volcano in Kamchatka, Russia. *Bull. Volcanol.* **80**, 33 (2018).
2. Sauerzapf, U., Lattard, D., Burchard, M. & Engelmann, R. The titanomagnetite-ilmenite equilibrium: New experimental data and thermo-oxybarometric application to the crystallization of basic to intermediate rocks. *J. Petrol.* **49**, 1161–1185 (2008).
3. Putirka, K. D. Thermometers and Barometers for Volcanic Systems. *Rev. Mineral. Geochemistry* **69**, 61–120 (2008).
4. Ganguly, J. & Tazzoli, V. Fe2+-Mg interdiffusion in orthopyroxene: retrieval from the data on intracrystalline exchange reaction. *Am. Mineral.* **79**, 930–937 (1994).
5. Morgan, D. J. *et al.* Time scales of crystal residence and magma chamber volume from modelling of diffusion profiles in phenocrysts: Vesuvius 1944. *Earth Planet. Sci. Lett.* **222**, 933–946 (2004).
6. Costa, F. & Morgan, D. *Time Constraints from Chemical Equilibration in Magmatic Crystals*. *Timescales of Magmatic Processes: From Core to Atmosphere* (John Wiley & Sons, Ltd, 2010). doi:10.1002/9781444328509.ch7.
7. Solaro, C. *et al.* A System Dynamics Approach to Understanding the deep Magma Plumbing System Beneath Dominica (Lesser Antilles). *Front. Earth Sci.* **8**, (2020).
8. Ostorero, L. *et al.* Time - window into the transcrustal plumbing system dynamics of Dominica (Lesser Antilles). *Sci. Rep.* **11**, 1–15 (2021).
9. Allan, A. S. R., Morgan, D. J., Wilson, C. J. N. & Millet, M.-A. From mush to eruption in centuries: assembly of the super-sized Oruanui magma body. *Contrib. to Mineral. Petrol.* **166**, 143–164 (2013).
10. Flaherty, T. *et al.* Multiple timescale constraints for high-flux magma chamber assembly prior to the Late Bronze Age eruption of Santorini (Greece). *Contrib. to Mineral. Petrol.* **173**, 75 (2018).
11. Smith, D. & Barron, B. R. Pyroxene-garnet equilibration during cooling in the mantle. *Am. Mineral.* **76**, 1950–1963 (1991).
12. Cherniak, D. J. & Dimanov, A. Diffusion in Pyroxene, Mica and Amphibole. *Rev. Mineral. Geochemistry* **72**, 641–690 (2010).
13. Carignan, J., Hild, P., Mevelle, G., Morel, J. & Yeghicheyan, D. Routine Analyses of Trace Elements in Geological Samples using Flow Injection and Low Pressure On-Line Liquid Chromatography Coupled to ICP-MS: A Study of Geochemical Reference Materials BR, DR-N, UB-N, AN-G and GH. *Geostand. Geoanalytical Res.* **25**, 187–198 (2001).